THE JOURNAL OF BIOLOGICAL CHEMISTRY
Vol. 276, No. 31, Issue of August 3, pp. 29233–29241, 2001
Printed in U.S.A.
© 2001 by The American Society for Biochemistry and Molecular Biology, Inc.

Hyperpolarization-activated Cyclic Nucleotide-gated Channel 1 Is a Molecular Determinant of the Cardiac Pacemaker Current I_f*

Received for publication, January 29, 2001, and in revised form, April 27, 2001
Published, JBC Papers in Press, April 27, 2001, DOI 10.1074/jbc.M100830200

Anna Moroni‡§¶, Luisa Gorza‖, Monica Beltrame, Biagio Gravante‡, Thomas Vaccari**, Marco E. Bianchi‡‡, Claudia Altomare‡, Renato Longhi§§, Catherine Heurteaux¶¶, Maurizio Vitadello‖, Antonio Malgaroli‡‡, and Dario DiFrancesco‡**

*From the ‡Dipartimento di Fisiologia e Biochimica Generali, the §Dipartimento di Biologia, and the **Dipartimento di Genetica e di Biologia dei Microrganismi, Università degli Studi di Milano, via Celoria 26, Milano 20133, the ‖Consiglio Nazionale delle Ricerche (CNR), Centro di Studio per la Biologia e Fisiopatologia Muscolare and Dipartimento di Scienze Biomediche Sperimentali, Università di Padova, via Trieste 75, Padova 35121, the ‡‡Dipartimento Ricerca Scientifica e Tecnologica (DIBIT), Istituto Scientifico San Raffaele (HSR), 20123 Milano, §§CNR, Istituto di Biocatalisi e Riconoscimento Molecolare, via M. Bianco 9, Milano 20131, Italy, and the ¶¶Institut de Pharmacologie Moléculaire et Cellulaire, Université de Nice Sophia Antipolis, 660 route des Lucioles, Sophia Antipolis, Valbonne 06560, France*

The pacemaker current I_f of the sinoatrial node (SAN) is a major determinant of cardiac diastolic depolarization and plays a key role in controlling heart rate and its modulation by neurotransmitters. Substantial expression of two different mRNAs (HCN4, HCN1) of the family of pacemaker channels (HCN) is found in rabbit SAN, suggesting that the native channels may be formed by different isoforms. Here we report the cloning and heterologous expression of HCN1 from rabbit SAN and its specific localization in pacemaker myocytes. rbHCN1 is an 822-amino acid protein that, in human embryonic kidney 293 cells, displayed electrophysiological properties similar to those of I_f, suggesting that HCN1 can form a pacemaker channel. The presence of HCN1 in the SAN myocytes but not in nearby heart regions, and the electrophysiological properties of the channels formed by it, suggest that HCN1 plays a central and specific role in the formation of SAN pacemaker currents.

The spontaneous electrical activity of mammalian heart arises from specialized myocytes of the cardiac sinoatrial node (SAN)[1] Early studies of the electrical properties of SAN myocytes have revealed the existence of a hyperpolarization-activated current, named I_f, important in the generation and autonomic control of the diastolic ("pacemaker") depolarization phase of the action potential (1). I_f is a mixed Na^+ and K^+ inward current, activated in the diastolic range of voltages (2, 3). Apart from its voltage sensitivity, I_f is also activated directly by intracellular cAMP (4), which acts by increasing the channel open probability. This mechanism underlies cardiac rhythm modulation by both sympathetic (β-adrenergic) (1) and parasympathetic (muscarinic) neurotransmitters (5). In addition to SAN pacemaker cells, the I_f current has been observed in other cardiac regions, such as Purkinje fibers, atrioventricular node, atrium and ventricle (6–8). Further, an I_f-like current (I_h current) has been recorded in several types of neurons (9, 10), where it controls cellular excitability.

A molecular characterization of I_f has recently become possible with the cloning of the hyperpolarization-activated cyclic nucleotide gated (HCN) channel family (11). This family comprises four members, HCN1–4, whose properties are similar to those of I_f and I_h channels (12–19).

HCN channels belong to the superfamily of voltage-gated potassium channels with six transmembrane domains and are likely to assemble in tetramers (11). The four isoforms differ in tissue localization and biophysical properties. HCN1, which is mainly expressed in the brain (12, 13), when heterologously expressed, displays properties of neuronal h-channels (fast activation kinetics, little dependence on cAMP (12)). On the other hand, HCN2 and HCN4, prominently expressed in heart as well as in brain (15–18), produce currents whose features are more reminiscent of the cardiac I_f (slower activation/deactivation kinetics and a more pronounced dependence on cAMP) and are therefore considered potential components of cardiac hyperpolarization-activated channels (19, 20). Although the expression of HCN1 mRNA has never been reported in total heart, a detailed analysis performed on rabbit cardiac SAN unexpectedly indicated expression of HCN1 (rbHCN1) mRNA in this tissue (21, 22) together with strong expression of HCN4 mRNA and traces of HCN2 mRNA (12, 18, 21). This coexpression raises the question as to if and to what extent each of the expressed isoforms contributes to the I_f current. The electrophysiological properties of HCN4 appear similar but not identical to those of I_f (18), suggesting that the native current is unlikely to be carried by HCN4 only. The activation kinetics of HCN4 (16, 18, 19), for example, is much slower than that reported for native I_f under similar experimental conditions (23–25). Similar considerations apply to HCN2, whose rather negative position of the activation curve, conductance properties, and cesium sensitivity together with evidence of extremely low levels of expression in the SAN, indicate that it also cannot

This is an open access article under the CC BY license.

* This work was supported by MURST and COFIN 1999 and 2000 grants (to A. Mo., L. G., and D. D.), Consiglio Nazionale delle Ricerche Grant 98.03045.CT04 (to L. G.), Giunta RegioneVeneto-Ricerca sanitaria finalizzata Grant 758/01/97 (to L. G.), INFM (to D. D.), and Telethon Grant 971 (to D. D.). The costs of publication of this article were defrayed in part by the payment of page charges. This article must therefore be hereby marked "*advertisement*" in accordance with 18 U.S.C. Section 1734 solely to indicate this fact.

The nucleotide sequence reported in this paper has been submitted to the GenBank™/EBI Data Bank with accession number AF168122 (rbHCN1).

¶ To whom correspondence should be addressed: Dipartimento di Fisiologia e Biochimica Generali, Sezione di Fisiologia Molecolare e Neurobiologia, via Celoria 26, Milano 20133, Italy. E-mail: anna.moroni@unimi.it.

[1] The abbreviations used are: SAN, sinoatrial node; HCN, hyperpolarization-activated cyclic nucleotide gated channel; rbHCN1, HCN1 from rabbit SAN; PCR, polymerase chain reaction; bp, base pair(s); mHCN1, mouse HCN1; ORF, open reading frame; uORF, upstream ORF; HEK, human embryonic kidney; CPT-cAMP, 8-(4-chlorophenylthio)-cAMP; PBS, phosphate-buffered saline; DAPI, 4,6-diamidino-2-phenylindole.

be solely responsible for the native channel (16, 20). On the other hand, electrophysiological parameters such as activation curve position and modulation by cAMP are extremely variable and may reflect differences in expression system, experimental conditions and protocols, as well as species differences. As a first approach, a comparison of the properties of the three individual isoforms 1, 2 and 4 with those of the native channel under similar experimental conditions, as well as isoform co-expression experiments, is required to investigate the subunit composition of native current. In the present work, HCN1 was cloned from rabbit SAN, and its electrophysiological characteristics were investigated by functional expression and compared with those of rabbit HCN4 (HAC4, 18) and native rabbit I_f recorded under similar conditions. Because the SAN is highly innervated by both sympathetic and vagal endings, we performed *in situ* hybridization experiments and immunolocalization to prove specific expression of HCN1 mRNA and protein in single pacemaker myocytes in order to exclude a neuronal origin for HCN1. The evidence that HCN1 is expressed in the SAN and the properties displayed by the channel in the heterologous system suggest that this isoform can contribute to the native current. Our investigation also indicates that the extent of the contribution by HCN1 may vary because the amount of functional protein appears to be under the control of translational and post-translational events. This implies the possibility of fine tuning of I_f current properties by modulation of the fractional contribution of different isoforms.

EXPERIMENTAL PROCEDURES

Tissue Source—New Zealand White rabbits weighing 0.8–1 kg were anesthetized by intramuscular injection of 4.6 mg/kg xylazine and 60 mg/kg ketamine and euthanized by cervical dislocation. The investigation conformed with guidelines for the care and use of laboratory animals as established by state and European directives as well as those of the U. S. National Institutes of Health.

Samples from different brain regions (cortex, cerebellum, thalamus plus hypothalamus), from different cardiac regions (atrial and ventricular myocardium, SAN node, and atrioventricular bundle) and from skeletal muscle were excised quickly, frozen immediately in liquid nitrogen, and stored at −80 °C until used.

Reverse Transcription-PCR, Library Screening, and 5′-Rapid Amplification of cDNA Ends—We cloned the first fragment of rbHCN1 by reverse transcription-PCR performed on rabbit SAN. Forty SAN preparations (corresponding to about 240 mg of tissue) were isolated from adult New Zealand rabbits in sterile and RNase-free conditions. Poly(A)$^+$ RNA was isolated using Fast Track (Invitrogen), treated with DNase, and retrotranscribed with oligo(dT) primer (Superscript preamplification system, Life Technologies, Inc.). PCR was performed (2 min at 95 °C, 35 times for 30 s at 95 °C, 30 s at 56 °C, and 1 min at 72 °C) on cDNA with the following oligonucleotides: 3FOR, 5′-GAGGARATMGTCAACTTCAACTG-3′ (corresponding to amino acids 448–455 of mBCNG1; Ref. 12) and 4REV, 5′-ATYTCGTTCTCCTGRTTGTT-3′ (corresponding to amino acids 604–610 of mBCNG1). The amplification product, 450 bp long, included the cyclic nucleotide binding region of rabbit HCN1 and was used to screen a cDNA library prepared from rabbit heart SAN regions (31). 5×10^5 phage clones of the cDNA library were hybridized at 65 °C with a mixture of two probes: the 450-bp fragment of rabbit HCN1 and a fragment containing the cyclic nucleotide binding region of human HCN2 (17) (nucleotides 1120–1660, GenBank AF065164). We retrieved and sequenced eight positive clones, all coding for rbHCN1, none of them full-length. The longest clone extended from the third transmembrane domain (S3) to the end, including 700 nucleotides of the 3′-untranslated region. We retrieved the 5′-end of rbHCN1 from SAN poly(A)$^+$ by reverse transcription-PCR. PCR was performed (2 min at 95 °C, 35 times for 30 s at 95 °C, 30 s at 54 °C, and 1 min at 72 °C) on cDNA with a forward primer designed on the 5′-untranslated region of mouse HCN1 (rbHCN1ATG 5′-GGTCGCGTCCTCCGGGC-3′) and a reverse primer designed in the S3-S4 linker of rbHCN1 (rbGSP3 5′-CTTGTAAACTTCTGAATCCCA-3′). The N terminus of rbHCN1 was about 120 nucleotides shorter than the mouse sequence. Translation of the full-length clone (Fig. 1) revealed the presence of a short upstream ORF (uORF) of 35 amino acids overlapping with the rbHCN1 ORF of 822 amino acids. The short uORF started with the first ATG (indicated as M1 in Fig. 1*b*), corresponding to the starting codon of mHCN1 and terminated with the stop codon TGA, downstream of the initiator codon of rbHCN1 ORF (indicated as M2 in Fig. 1*b*). The uORF showed high similarity to mHCN1 (27 out of 35 amino acids are identical). The nucleotide sequence around M1 was in agreement with the Kozak consensus sequence (A/GCCATGG) (26). The nucleotide sequence around M2, inside the short uORF, was also in good agreement with the Kozak consensus sequence. M2 started, with a frame +1 with respect to M1, the main ORF of 822 amino acids corresponding to rbHCN1 (Fig. 1). Downstream of the stop codon of the uORF there was a third ATG (we refer to this ATG as M3 in Fig. 1*b*), which starts (in-frame with M2) a 793-amino acid ORF, which we called ΔNrbHCN1, corresponding to a truncated form of rbHCN1, lacking the first 29 amino acids at the N terminus. The sequence around this ATG showed no similarities to the Kozak consensus sequence.

To confirm these sequence data and to exclude the occurrence of post-transcriptional modifications, such as RNA editing (27), we amplified the 5′-end of HCN1 from rabbit genomic DNA (primer forward rbHCN1ATG 5′-ggtcgcgtcctccgggc-3′; primer reverse rbGSP5 5′-tgcggagggagaatttgttga; 96 °C × 45 s, 56 °C × 1 min, 72 °C × 2 min). The genomic sequence, identical to the cDNA sequence, confirmed the presence of the 35-amino acid uORF overlapping with rbHCN1 ORF and proved the absence of introns in the first part of the sequence, from M1 to amino acid +20 downstream of M3.

Constructs M1, M2, and M3—For heterologous expression we prepared construct M1 by subcloning the full-length channel in the *Eco*RV restriction site of the polylinker of the mammalian expression vector pCDNA 3.1 (Invitrogen). Construct M2 was prepared by PCR (ΔNM1ATGfor 5′-ttaagcttacgatggcaacagtcttcc-3′, rbGSP1rev 5′-ccaggaatcattaaccatttc-3′) obtaining a 600-nucleotide band that excluded the first ATG M1 and then ligating it at the 5′ of construct M1 by means of the polylinker site *Hin*dIII of pCDNA 3.1 and *Nde*I site of rbHCN1. Construct M3 was prepared from construct M1 by means of the restriction site *Ksp*I some 20 nucleotides upstream of the third ATG, M3. The nucleotides surrounding the initiator codon of each construct were preserved so as not to perturb the native Kozak (M1 and M2) or non-Kozak sequences.

Electrophysiology—For functional expression each construct was co-transfected with a plasmid containing green fluorescent protein into modified HEK 293 (Phoenix) cells (28). The cells were transiently transfected according to a standard calcium phosphate protocol, as described previously (20).

Experiments were performed on cells incubated after transfection at 37 °C in 5% CO_2 for 1–5 days. On the day of the experiment cells were dispersed by trypsin, plated at a low density on 35-mm plastic Petri dishes, and allowed to settle for 2 to 4 h; dishes were then placed on the stage of an inverted microscope and single cells patch clamped in the whole cell configuration according to standard methods (25). Cells were perfused at room temperature (24–26 °C) with a control Tyrode solution containing (in mM): NaCl, 140; KCl, 5.4; $CaCl_2$, 1.8; $MgCl_2$, 1; D-glucose, 5.5; Hepes-NaOH, 5 (pH = 7.4). In pilot experiments run in untransfected cells we found that a significant fraction of the endogenous current of HEK 293 (Phoenix) cells was reduced by the addition of K^+ and Ca^{2+} channel blockers such as $BaCl_2$ (1 mM), $MnCl_2$ (2 mM), $NiCl_2$ (100 μM), and nifedipine (20 μM). We did not explore the nature of these endogenous components, but because the blockers used do not affect the I_f pacemaker current and are commonly used in experiments on native channels (29), they were added routinely to standardize measurements. The solution was delivered via a fast flow perfusion pipette, positioned on top of the cell under study, which allowed rapid (<1 s) solution changes.

Whole-cell pipettes were filled with an intracellular-like solution containing (mM): NaCl, 10; KCl, 130; EGTA, 1.0, Hepes-KOH, 5; $MgCl_2$, 0.5; ATP (sodium salt), 2; GTP (sodium salt), 0.1; phosphocreatine, 5 (pH = 7.2). To investigate cesium- and cyclic nucleotide-dependent effects on the rbHCN1 current, we performed experiments in the whole cell configuration perfusing external solution with CsCl (5 mM) and CPT-cAMP (100 μM).

Electrophysiological measurements were also performed, under the same experimental conditions, on HEK 293 cells transfected with mHCN1 (BCNG1, according to Clapham (11), GenBank AF028737, kindly provided by Bina Santoro, Columbia University, New York), rabbit HAC4 (HCN4, according to Clapham (11) GenBank AB022927, kindly provided by H. Ohmori, University of Kyoto), and on isolated rabbit SAN myocytes (25).

Data Analysis—Activation curves were obtained by standard two-step voltage clamp protocols employed previously for analysis of I_f current in SAN cells (25). The protocols consisted of hyperpolarizations

a

```
mHCN1   MEGGGKPNSASNSRDDGNSVFPSKAPATGPVAADKRLGTPPRGGAAGKEHGNSVCFKVDGGGGEEPAGSFEDAEGPRRQYGFMQRQFTSMLQPGVNKFSLRMFGSQKAVEKEQERVKTAG 120
rbHCN1                  MATASSPPRRPRRARG-------------------------------------LEDAEGPRRQYGFMQRQFTSMLQPGVNKFSLRMFGSQKAVEKEQERVKTAG  67
uORF    MEGGGKPNSSSNSRDDGNSVFPAKAPATGAGPGGR*                                                                                  35

                    S1                                  S2                                                  S3
mHCN1   FWIIHPYSDFRFYWDLIMLIMMVGNLVIIPVGITFFTEQTTTPWIIFNVASDTVFLLDLIMNFRTGTVNEDSSEIILDPKVIKMNYLKSWFVVDFISSIPVDYIFLIVEKGMDSEVYKTA 240
rbHCN1  FWIIHPYSDFRFYWDLIMLIMMVGNLVIIPVGITFFTEQTTTPWIIFNVASDTVFLLDLIMNFRTGTVNEDSSEIILDPKVIKMNYLKSWFVVDFISSIPVDYIFLIVEKGMDSEVYKTA 187

                    S4                                  S5                                                  P
mHCN1   RALRIVRFTKILSLLRLLRLSRLIRYIHQWEEIFHMTYDLASAVVRIFNLIGMMLLLCHWDGCLQFLVPLLQDFPPDCWVSLNEMVNDSWGKQYSYALFKAMSHMLCIGYGAQAPVSMSD 360
rbHCN1  RALRIVRFTKILSLLRLLRLSRLIRYIHQWEEIFHMTYDLASAVVRIFNLIGMMLLLCHWDGCLQFLVPLLQDFPPDCWVSLNEMVNDSWGKQYSYALFKAMSHMLCIGYGAQAPVSMSD 307

                    S6
mHCN1   LWITMLSMIVGATCYAMFVGHATALIQSLDSSRRQYQEKYKQVEQYMSFHKLPADMRQKIHDYYEHRYQGKIFDEENILSELNDPLREEIVNFNCRKLVATMPLFANADPNFVTAMLSKL 480
rbHCN1  LWITMLSMIVGATCYAMFVGHATALIQSLDSSRRQYQEKYKQVEQYMSFHKLPADMRQKIHDYYEHRYQGKIFDEENILNELNDPLREEIVNFNCRKLVATMPLFANADPNFVTAMLSKL 427

                    CNBD
mHCN1   RFEVFQPGDYIIREGAVGKKMYFIQHGVAGVITKSSKEMKLTDGSYFGEICLLTKGRRTASVRADTYCRLYSLSVDNFNEVLEEYPMMRRAFETVAIDRLDRIGKKNSILLQKFQKDLNT 600
rbHCN1  RFEVFQPGDYIIREGAVGKKMYFIQHGVAGVITKSSKEMKLTDGSYFGEICLLTKGRRTASVRADTYCRLYSLSVDNFNEVLEEYPMMRRAFETVAIDRLDRIGKKNSILLQKFQKDLNT 547

mHCN1   GVFNNQENEILKQIVKHDREMVQAIPPINYPQMTALNCTSSTTPTSRMRTQSPPVYTATSLSHSNLHSPSPSTQTPQPSAILSPCSYTTAVCSPPIQSPLATRTFHYASPTASQLSLMQ 720
rbHCN1  GVFNNQENEILKQIVKHDREMVQAIAPISYPQMTALNSTSSTATPTSRMRTQSPPVYTATSLSHSNLHSPSPSTQTPQPSAILSPCSYTTAVCSPPVQSPLATRTFHYASPTASQLSLM- 666
                                  ○  ○          ○        ○○            ○ ○   ○ ○    ○        ○○  ○          ○

mHCN1   QPQQQLPQSQVQQTQTQTQQQQQQQQQQQQQQQQQQQQQQQQQQQQQQQQQQQQQQQQPQTPGSSTPKNEVHKSTQALHNTNLTKEVRPLSASQPSLPHEVSTLISRPHPTVGESLASIPQPV 840
rbHCN1  -PQ----------------QQQQPQAPQTQ----------------PQQPPQQPQTPGSATPKNEVHKSTQALPNTSLTREVRPLSASQPSLPHEVSTLISRPHPTVGESLASIPQPV 751
         ○                        ●  ●                 ●  ●●  ○  ○    ○          ●        ○    ○  ○        ○○        ○ ○

mHCN1   AAVHSTGLQAGSRSTVPQRVTLFRQMSSGAIPPNRGVPPAPPPPAA-VQRESPSVLNTDPDAEKPRFASNL* 910
rbHCN1  AAVHSAGLQAAGRSTVPQRVTLFRQMSSGAIPPNRGVPPAPPPPAAPLQREASSVLNTDPEAEKPRFASNL* 822
                        ○            ○○   ○○○○○○ ●          ○   ○
```

b

```
        M1 uORF                                                  M2 rbHCN1
ccgggcatggaaggaggcggcaagcccaactcttcgtccaacagccgggacgatggcaacagcgtcttccccgccaaggcgcccg  85
       M  E  G  G  G  K  P  N  S  S  S  N  S  R  D  D  G  N  S  V  F  P  A  K  A  P    26
                                                     M  A  T  A  S  S  P  P  R  R  P    11

                                                          M3 ΔNrbHCN1
cgacgggcgcggggcctggaggacgctgaggggccgcggcggcagtacggcttcatgcagcgacagttcacctccatgctgcagc 170
A  T  G  A  G  P  G  G  R  *                                                             35
 R  R  A  R  G  L  E  D  A  E  G  P  R  R  Q  Y  G  F  M  Q  R  Q  F  T  S  M  L  Q     39
```

c

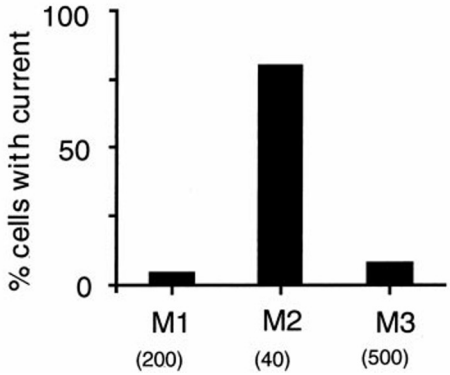

FIG. 1. *Panel a*, protein alignment of mHCN1 (GenBank AF028737) and rbHCN1 (GenBank AF168122). The short uORF, partly overlapping rbHCN1, is also reported (*boxed*) to show its homology to mHCN1. Identical residues between mHCN1 and rbHCN1 are *highlighted* in *gray*. *Dots* indicate gaps. *Asterisks* indicate stop codons. The six putative transmembrane segments (*S1–S6*), the pore region (*P*), and the cyclic nucleotide binding domain (*CNBD*) of HCN1 are indicated (——). *Open* (○) and *closed circles* (●) indicate conserved and additional prolines, respectively, in the C terminus of rbHCN1 compared with the mouse clone. *Panel b*, nucleotide sequence of the 5′-end of rbHCN1 cDNA. The first three starting codons atg (*bold*) are *underlined* and named M1–M3. An *asterisk* indicates the stop codon (tga, *underlined*) of the uORF. Translation of the nucleotide sequence from the first ATG (M1) predicts the short uORF of 35 amino acids, partly overlapping with rbHCN1. Translation starting from the second ATG (M2), which is found inside and not in-frame with the short uORF, predicts the 822-amino acid ORF of rbHCN1. Also indicated is the truncated form (ΔNrbHCN1) starting from the third ATG (M3), which codes for an ORF of 793 amino acids. *Panel c*, effect of deletion and/or disruption of the uORF on the expression rate of rbHCN1 current in HEK 293 cells. Cells were transfected with the three constructs that included (M1), disrupted (M2), and excluded (M3) the uORF (see *panel b*) and tested by patch clamp in the whole cell configuration. The number of cells endowed with hyperpolarization-activated, time-dependent, cesium-sensitive current is reported for each construct. The total number of cells tested for each construct is reported in *brackets*.

applied in 10-mV steps from a fixed holding potential of −35 mV followed by a step to the test voltage (−125 mV) where the amplitude of the activation current tails was measured. The amplitudes at −125 mV, normalized to the maximum level, yielded the activation variable ($(I_{MAX} - I)/I_{MAX}$ = fractional activation). Experimental data were fitted by a Boltzmann function $y = (1/(1 + \exp((V - V_{1/2})/s))$ where y = fractional activation, V = voltage, $V_{1/2}$ = half-activation voltage, and s = inverse slope coefficient.

To account for the voltage dependence of the activation time constant (see Fig. 2), the duration of the activation steps depended on the test voltage and was selected to allow steady-state activation to be reached. Activation traces at different voltages were fitted by single exponential curves after an initial delay. Shifts of the activation curve caused by cAMP were obtained by applying hyperpolarizing steps at a fixed frequency (1/6 Hz) and compensating the current increase during CPT-cAMP perfusion by changing manually the holding potential (30).

Northern Blot Analysis—A Northern blot with 2–4 μg of poly(A)$^+$ RNA from rabbit tissues was hybridized, at 65 °C, with a ^{32}P-labeled cDNA probe corresponding to rabbit 3′-end (380 bp long, including 175 nucleotides of 3′-untranslated region). The filter was washed with 2 × SSC, 0.5% SDS (2 × 15 min at 65 °C), 1 × SSC, 0.5% SDS (1 × 15 min at 65 °C), 0.1 × SSC, 0.5% SDS (1 × 15 min at room temperature) and exposed to x-ray film at −80 °C with an intensifying screen for 10 days. Normalization was performed with murine glyceraldehyde-3-phosphate dehydrogenase. Filters were stripped between subsequent hybridizations by pouring boiling 0.5% SDS on them.

In Situ Hybridization—For *in situ* hybridization, ^{35}S-radiolabeled antisense and sense cRNA probes were transcribed *in vitro* from rbHCN1 cDNA and hybridized on cryostat sections following procedures described previously (31). In brief, radiolabeled antisense and sense cRNA probes were transcribed from the cDNA clone corresponding to the 3′-end of the rbHCN1 mRNA (the same probe used previously for Northern blot analysis; see above) after linearization with *Bam*HI or *Kpn*I (Promega), respectively, using T7 or T3 RNA polymerase (Epicentre) and ^{35}S-labeled-UTP. Both probes corresponded to the length of the insert (380 bp), and for *in situ* hybridization purposes they were digested to 100 nucleotides by mild alkaline hydrolysis. Cryosections (10 μm thick) were fixed with formaldehyde and digested with 20 μg/ml proteinase K. Sections were hybridized overnight at 52 °C with 20 μl of probe at a concentration of 1 × 10^5 cpm/μl and washed at 65 °C with 50% formamide, 0.3 M NaCl, 0.03 M sodium citrate, and 0.1 M dithiothreitol. After dehydration sections were dipped in autoradiographic emulsion (Kodak NTB-2), diluted 1:1 with water, and exposed for 25 days at 4 °C. Slides were developed with D19 (Kodak) for 3.5 min, fixed, and examined with a Zeiss Axioplan microscope equipped with dark field optics.

Immunochemistry—Polyclonal antibodies anti-HCN1 (αHCN1) were obtained by injecting into a rabbit a PBS solution of keyhole limpet hemocyanin-conjugated peptide of 19 amino acids (STLISRPHPTVGESLASIP, amino acids 819–837 in the C terminus of mHCN1 (12)), diluted 1:1 with Freund's adjuvant. A cysteine residue was added to the peptide sequence to allow further purification of the antibody on an Affi-Gel 102 (Bio-Rad) column by means of the cross-linking reagent Sulfo-SMCC (Pierce).

The specificity of the anti-neurofilament monoclonal antibody iC8, which identifies the M subunit of neurofilaments expressed in rabbit conduction system myocytes, has been described previously (32).

Secondary anti-rabbit and anti-mouse polyclonal antibodies coupled to horseradish peroxidase were from Bio-Rad and Dakopatts, respectively. Fluorescein-conjugated anti-mouse antibodies were from Dakopatts. Rhodamine-conjugated donkey anti-rabbit antibodies were from Sigma.

For Western blot analysis with αHCN1, protein extracts of brain regions and SAN were separated by 10% SDS-polyacrylamide gel electrophoresis and electroblotted onto nitrocellulose membranes (Schleicher & Schuell). Blocking and antibody incubations were carried out in Blotto solution (50 mM Tris, pH 7.4, 150 mM NaCl, 0.1% Tween 20, 5% powdered skimmed milk). αHCN1 was used at a 1:500 dilution. Secondary anti-rabbit antibodies coupled to horseradish peroxidase (Bio-Rad) were used at a 1:5,000 dilution and the bands visualized by incubation in ECL Western blotting detection reagents (Amersham Pharmacia Biotech). For immunocytochemistry, cryosections serial to those processed for *in situ* hybridization were incubated with the anti-neurofilament antibody iC8, diluted 1:1,000 with 0.5% bovine serum albumin in PBS to identify heart conduction system myocytes (32). Incubation was carried out in a humidified chamber at room temperature for 30 min. After three 10-min rinses in PBS, sections were incubated with appropriate dilutions of secondary antibodies coupled with peroxidase, and antibody binding was revealed using diaminobenzidine as a substrate.

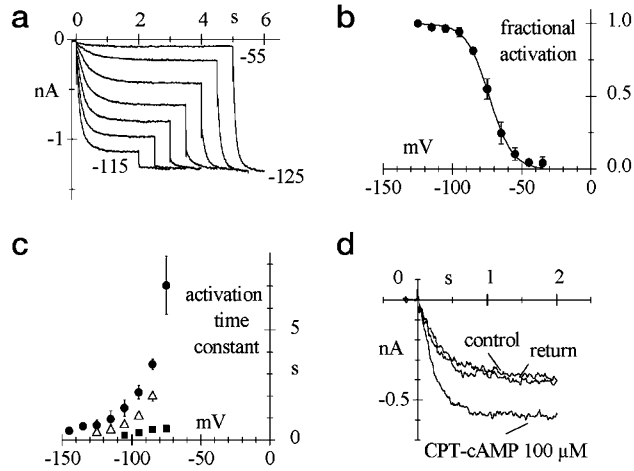

FIG. 2. **Electrophysiological properties of the expressed rbHCN1 channel and comparison with activation kinetics of rbHCN4 and native I_f channel of rabbit SAN myocytes.** *Panel a*, rbHCN1 channel currents elicited by an activation curve protocol from a holding potential of −35 to −115 mV in 10-mV increments followed by a step to −125 mV. The duration of the activation steps depended on the test voltage and was selected to allow steady-state activation to be reached. *Panel b*, activation curve of rbHCN1 obtained from averaging values from $n = 3$ cells. Tail currents recorded at −125 mV (as shown in *panel a*) were normalized and plotted as a function of the preceding conditioning voltage. Fitting exponential data points by a Boltzmann function (fractional activation = $1/(1 + \exp((V - V_{1/2})/s))$) yielded a half-activation voltage $V_{1/2} = -73.4 \pm 0.36$ mV and an inverse slope factor $s = 8.12$ mV. *Panel c*, voltage dependence of activation kinetics. Activation traces at different voltages were fitted by single exponential curves after an initial delay, and the resulting time constants were plotted as a function of conditioning voltage. Data from rbHCN1 (*filled squares*, $n = 8$) and rbHCN4 (HAC4, 18) (*filled circles*, $n = 2$) channels in transfected cells and native (*open triangles*, $n = 7$) channels (I_f) in SAN myocytes were obtained under the same experimental conditions (room temperature, 24–26 °C). *Panel d*, modulation of rbHCN1 current by CPT-cAMP. Currents were evoked by clamping from a holding potential of −35 to −95 mV. Traces were recorded in the absence and in the presence of 100 μM CPT-cAMP in the external solution.

For immunofluorescence, rabbit SAN cells were isolated by enzymatic digestion (25) and plated onto a glass coverslip by centrifugation (cytospin, 1′ × 1,000 rpm). The cells were then fixed (4% paraformaldehyde or acetone as indicated), quenched (0.1 M glycine in PBS), blocked (1% bovine serum albumin, 0.4% saponin in PBS), and exposed either to αHCN1 antibodies diluted 1:100 in blocking solution or to anti-neurofilament NF-M antibody (whereas control cells were exposed only to blocking buffer). After washing in blocking solution, both control and treated cells were incubated with appropriate dilution of fluorescein- or rhodamine-conjugated secondary antibodies. The samples were mounted with Vectashield mounting medium with DAPI (Vector).

The images were acquired (with the same parameters for control and treated cells) by confocal microscopy (Leica TCS NT) using argon/krypton (for rhodamine) and argon (for DAPI) lasers.

RESULTS

Rabbit HCN1—rbHCN1 is an 822-amino acid protein with six predicted transmembrane domains, a pore region, and a cyclic nucleotide binding domain in the C terminus. It is almost identical to mHCN1 in the transmembrane regions and the cyclic nucleotide binding domain, but it has shorter cytoplasmic N and C termini. The N terminus of rbHCN1 cDNA is shorter by about 120 nucleotides, which represents a high GC-rich sequence in mouse; rbHCN1 also lacks the CAG repeats corresponding to the long stretch of glutamines (poly(Q)) found in the cytoplasmic C terminus of the mouse clone (Fig. 1*a*).

Heterologous Expression of rbHCN1 in 293 Cells—We prepared for heterologous expression three different constructs including (construct M1), disrupting (construct M2), and excluding (construct M3) the 35-amino acid uORF overlapping

TABLE I

Comparison of the properties of heterologously expressed rbHCN1 and rbHCN4 channels with native rabbit SAN I_f

rbHCN1 and rbHCN4 channels were expressed in HEK 293 cells. Native I_f was measured in isolated rabbit SAN myocytes (for methods, see Ref. 25). All experiments were performed at room temperature (24–26 °C). Half-activation voltage ($V_{½}$) and time constants of activation data were obtained in the whole cell configuration. Modulation of rbHCN1 by cAMP was measured in whole cell conditions by the addition of 100 μM CPT-cAMP to the external solution; modulation by cAMP of rbHCN4 and native I_f was measured on macropatches by superfusion of the intracellular patch side with 10 μM cAMP.

	$V_{½}$	Activation time constant at −95 mV	cAMP-induced shift
	mV	*ms*	*mV*
rbHCN1	−73.4 ± 0.4 (n = 3)	322 ± 46 (n = 8)	6.7 ± 0.3 (n = 4)
rbHCN4	−81.4 ± 0.6 (n = 5)	2,159 ± 304 (n = 2)	16.3 ± 1.3 (n = 6)
Rabbit SAN I_f	−65.9 ± 1.6 (n = 4)	1,068 ± 109 (n = 7)	10.2 ± 0.2 (n = 39)[a]

[a] Ref. 45.

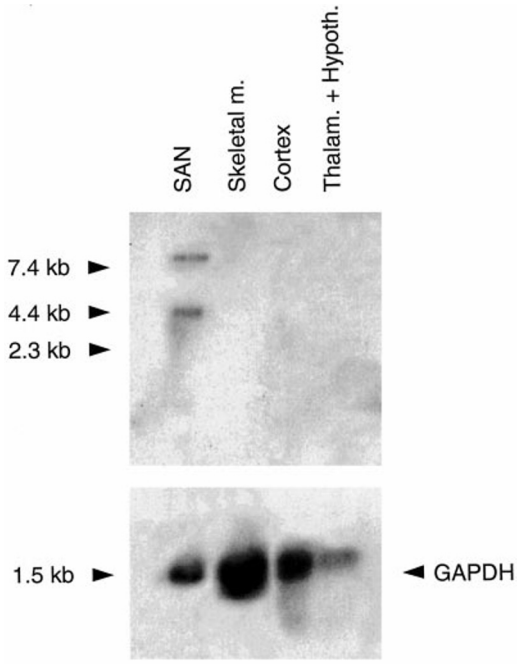

FIG. 3. **Northern blot analysis of HCN1 expression in different rabbit tissues.** Two μg of poly(A)$^+$ RNA, isolated from SAN, skeletal muscle, cortex, and thalamus plus hypothalamus, was loaded. The filter was probed with a DNA fragment of 380 bp in the 3′-untranslated region of rbHCN1. The positions of molecular mass standards are shown on the *left*. Glyceraldehyde-3-phosphate dehydrogenase (*GAPDH*) was used as an internal control to check quantity and integrity of loaded RNA.

the starting ATG codon of rbHCN1 cDNA (see "Experimental Procedures" and Fig. 1*b*).

Fig. 1*c* shows the percentage of cells expressing hyperpolarization-activated, cesium-sensitive, current when tested by patch clamp. Construct M1, which included the complete uORF, showed the lowest percentage. We measured a current activated in hyperpolarization, blocked by cesium, in 8 out of 200 fluorescent cells tested (4%). Construct M2, which included a disrupted uORF and started translation from M2, the initiator codon of the 822-amino acid ORF of rbHCN1, showed a very high percentage: in 32 out of 40 fluorescent cells tested (80%) we found a hyperpolarization-activated current that was blocked by cesium. Construct M3 excluded the uORF and translated a 793-amino acid ORF that we considered a truncated form of rbHCN1 (ΔNrbHCN1). This construct caused expression of cesium-sensitive, hyperpolarization-activated current in a very low percentage of cells: 40 out of 500 cells (8%).

It should be noted that subsequent analysis of currents showed no differences in the biophysical properties of the expressed channels, and therefore Fig. 2 and Table I include measurements obtained with all constructs.

Properties of Expressed rbHCN1 Channels—To investigate the biophysical properties of the rbHCN1 current we applied, in the whole cell configuration, standard voltage clamp protocols to HEK 293 cells expressing rbHCN1. Hyperpolarizing steps applied from a holding potential of −35 mV to the range −45 to −125 mV elicited an inward current that was blocked by 5 mM cesium (not shown). This current was absent in mock experiments where the cells were transfected with an empty vector (not shown).

A typical set of currents elicited by an activation curve protocol (see "Experimental Procedures") is shown in Fig. 2*a*. The mean activation curve obtained by averaging n = 3 cells is shown in Fig. 2*b*. The current has a threshold of about −40 mV and is fully activated at about −110 mV. Fitting exponential data points by a Boltzmann function yielded a half-activation voltage of −73.4 ± 0.4 mV and an inverse slope factor of 8.1. In Fig. 2*c*, mean time constants of activation measured by fitting activation records in the voltage range −75 to −125 mV with single exponential time course are plotted. For a comparison, Fig. 2*c* also shows the time constants of activation measured by fitting rbHCN4 (18) and native I_f (from SAN myocytes) currents recorded under the same conditions. The kinetics of the native channel was clearly intermediate between those of rbHCN4 and rbHCN1, the two main isoforms of rabbit SAN.

Fig. 2*d* shows the effect of cAMP on current amplitude and kinetics. Perfusion with 100 μM membrane-soluble cAMP agonist CPT-cAMP in the whole cell configuration yielded an increase in current amplitude and acceleration of the activation kinetics. The shift of the current activation curve measured in the example of Fig. 2*d* was 6.6 mV, and the average shift in n = 4 cells was 6.7 ± 0.28 mV (n = 4). Table I summarizes for comparison the properties of rbHCN1, rbHCN4, and rabbit SAN I_f. Half-activation voltages ($V_{½}$) slightly differ between the two isoforms and in both cases appear more negative than in the native channel, which may reflect differences in cAMP concentrations between HEK 293 and SAN cells. Time constants of activation (1,068 ms) and cAMP-induced shift (10.21 ± 0.2 mV) of native I_f are clearly intermediate between those measured for rbHCN1 (322 ± 46 ms, 6.7 ± 0.3 mV) and rbHCN4 (2,159 ± 304 ms, 16.3 ± 1.3 mV).

Expression of rbHCN1 mRNA in SAN—We evaluated the expression of rbHCN1 in SAN tissue by Northern blotting. Fig. 3 shows a positive signal in SAN poly(A)$^+$ but not in skeletal muscle and two different brain regions (cortex and thalamus plus hypothalamus). The probe specifically recognized two bands of 4.4 and >7.4 kilobases, respectively, similar to that reported for mHCN1 in the brain (12). By further analyzing other rabbit tissues we obtained a positive signal for hippocampus and cerebellum in which we observed a single transcript >7.4 kilobases long (data not shown).

rbHCN1 mRNA Accumulates in Myocytes of the SAN—*In situ* hybridization experiments were undertaken to explore rbHCN1 mRNA distribution at the cellular level. Sections from

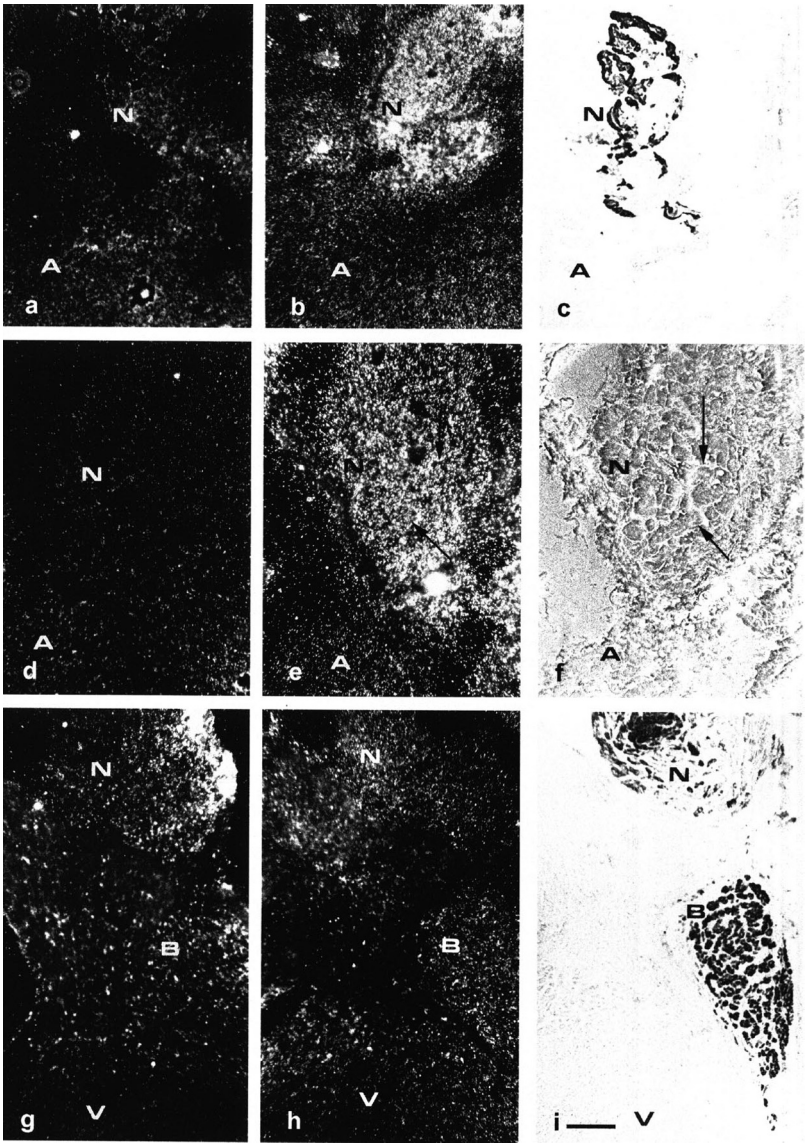

FIG. 4. **RbHCN1 mRNA expression in rabbit heart conduction system myocytes.** Serial consecutive cryostat sections of the rabbit SAN region (*panels a–f*) and atrioventricular node and bundle region (*panels g* and *h*) were used. Dark field micrographs show hybridization with sense RbHCN1 cRNA probe (*panels a*, *d*, and *g*) and antisense probe (*panels b*, *e*, and *h*). *Panels c* and *i* correspond to bright field micrographs of peroxidase immunostaining with the anti-neurofilament antibody iC8, which decorates conduction system myocytes of the SAN and atrioventricular nodes (*N*) and atrio-ventricular bundle (*B*). *Panel f* shows a phase contrast micrograph of the same field illustrated in *panel e*. Note that a high concentration of silver grains is detectable only in the SAN region (*panels b* and *e*, *N*) and is concentrated within myocytes (*panel e* and *f*, *arrows*); conduction system myocytes of the atrioventricular node and bundle display weaker hybridization signals (*panel h*, *N* and *B*), similar to working atrial (*A*) and ventricular (*V*) myocytes (*panels b*, *e*, and *f*). *Bar*, *panels a–c*, *g*, and *h*, 150 μm; *panels d–f*, 75 μm.

rabbit cerebellum were used to confirm rbHCN1 mRNA localization in neuronal cells. The antisense rbHCN1 probe showed diffuse positive hybridization signals in the granule cell layer and in the Purkinje neuron bodies, whereas only weak signals were observed in the molecular layer compared with background signals displayed by hybridization with the sense probe (data not shown).

In the heart, the same antisense probe showed low signals of hybridization in cardiomyocytes, whereas only background hybridization signals were detectable in non-muscle cardiac cells, as shown by comparison with signals obtained after hybridization with the sense probe (compare regions marked as *A* and *V* in Fig. 4).

Analysis of antisense signal localization in heart regions enriched in conduction system myocytes revealed a dual pattern of distribution. Myocytes of the SAN, identified using the expression of the neurofilament M subunit as a marker for rabbit conduction system myocytes (31, 32, and Fig. 4, *panel c*), showed hybridization signals for antisense rbHCN1 cRNA which were stronger than in the surrounding working atrial myocytes (Fig. 4, *panels b* and *e*). The myocyte nature of the cells accumulating rbHCN1 mRNA was further confirmed by combining dark field and phase contrast observations at higher magnification (Fig. 4, *panels e* and *f*, *arrows*). Conversely, conduction system myocytes of the atrioventricular bundle did not reveal any differences in rbHCN1 accumulation with respect to either working ventricular or atrial myocytes (Fig. 4, *panel h*).

rbHCN1 Protein—To characterize the protein encoded by rbHCN1 we generated antibodies against a peptide in the predicted cytoplasmic C terminus. In Western blots of mouse hippocampal extracts, αHCN1 specifically recognized a double band with apparent molecular masses of about 130 and 110 kDa (Fig. 5*a*), which is consistent with the 132-kDa band reported previously by Santoro *et al.* (12) in mouse brain.

The lower band recognized by our antibody in mouse hippocampus could represent a different glycosylated form of the higher band (see Ref. 12). Preadsorbing the antibody with the antigenic peptide completely abolished the labeling (*lane Ab+P*, Fig. 5*a*), thus indicating that the bands recognized by the antibody do represent the native HCN1 subunit. In protein extracts of HEK 293 cells transfected with HCN1 (construct M3), the antibody recognized a broad band with an apparent molecular mass of about 97 kDa, which was absent in control cells (Fig. 5*b*). This lower molecular mass corresponds to the shorter cDNA sequence of this construct (ΔNrbHCN1) compared with mHCN1 and may also correspond to a different glycosylated form of the protein in HEK 293 cells (12).

Fig. 6 shows a Western blot analysis performed on rabbit SAN, rabbit hippocampus, and for comparison, mouse hippocampus.

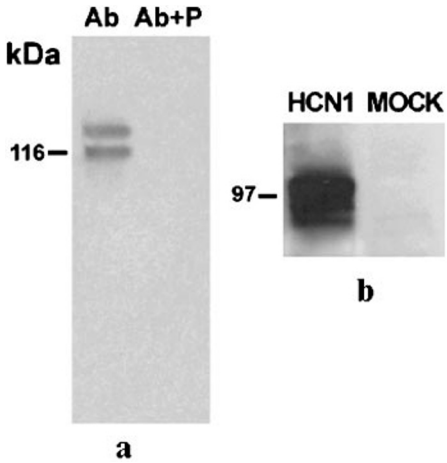

FIG. 5. **Western blot analysis of HCN1 protein.** *Panel a*, 30 μg of mouse hippocampus proteins was loaded in each lane and probed with αHCN1 (*Ab*) and αHCN1 preadsorbed with the keyhole limpet hemocyanin-coniugated peptide (*Ab+P*). *Panel b*, 30 μg of proteins from HEK 293 cells transfected with rbHCN1 (construct M3) and 50 μg of control HEK 293 cells (mock transfected) were loaded in each lane and probed with αHCN1.

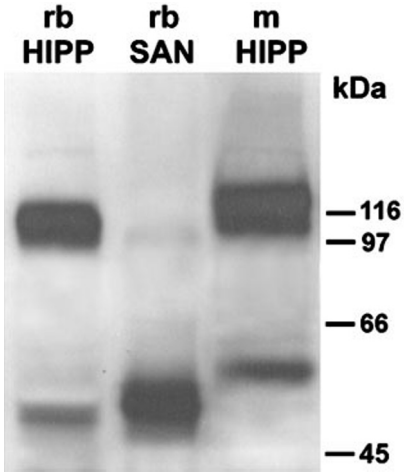

FIG. 6. **Western blot analysis of HCN1 protein in different tissues.** Thirty μg of proteins was loaded per strip and then probed with αHCN1. rbHIPP, rabbit hippocampus; rbSAN, rabbit SAN; and mHIPP, mouse hippocampus.

The antibody recognized a strong diffuse band in the hippocampus and a faint band in the SAN at a molecular mass higher than 97 kDa. At shorter exposure times a double band was clearly visible in rabbit and mouse hippocampus (data not shown). In SAN extracts, even with prolonged exposure times, a double band was never observed. It is worth noting that the antibody recognized a 50-kDa band in rabbit and a slightly higher molecular mass band in mouse. This band appeared stronger in SAN than in hippocampus and may represent a pattern of protein degradation. Because αHCN1 recognizes a peptide in the C terminus of HCN1, this band corresponds roughly to the C-terminal half of the protein, the cytoplasmic domain downstream of the six transmembrane segments.

HCN1 Protein Is Expressed in SAN Myocytes—To demonstrate that HCN1 is specifically expressed in SAN myocytes and that its presence in our preparation is not caused by a contamination of the surrounding nervous system we performed immunolocalization on single pacemaker myocytes obtained by enzymatic dispersion of rabbit SAN region.

Fig. 7, *panel a*, shows a typical pacemaker myocyte obtained from this tissue. The central "leading" SAN myocytes are roughly spindle-shaped, having a middle wider portion with the nucleus and two thinner endings slightly bent in a croissant-like shape. They showed typical cytological features such as rare and disordered striations and large vacuoles. The contractile system was extremely poorly developed and was less axially oriented than in atrium cells (33). It has been described previously that the majority of rabbit SAN cells, but not atrial myocytes, reacted with anti-neurofilament NF-L antibody (34). We found that a large proportion of spindle-like SAN cells in our preparation reacted with anti-neurofilament NF-M antibody iC8. Fig. 7, *panel b*, shows a typical example. When treated with αHCN1 (Fig. 7, *panel d*), SAN spindle-like myocytes showed discrete areas of labeling or hot spots, a type of distribution that agrees with previous reports based on single channel recordings for the I_f channel (see Ref. 2). A myocyte not treated with αHCN1 is shown in *panel c* for comparison. The *blue circle* corresponds to the DAPI-stained nucleus of the underlying myocyte.

DISCUSSION

The hyperpolarization-activated channel HCN1 has been identified previously in mouse brain as the isoform that codes for the neuronal current $I_{h,}$ in agreement with its mRNA expression pattern (12, 13, 15). Although expressed predominantly in neuronal tissue, HCN1 is also present in SAN (21, 22). Here we have cloned HCN1 cDNA from cardiac SAN, expressed it in HEK 293 cells, and have shown that HCN1 mRNA and protein localize specifically in the pacemaker myocytes.

rbHCN1 protein is almost identical to mHCN1 in the transmembrane segments and cyclic nucleotide binding domain but diverges from it in the cytoplasmic N and C termini, which are shorter. However, the proline-rich SH3 ligand sequence found at the C terminus of mHCN1 was conserved in rabbit (Fig. 1*a*). This sequence has been shown to interact directly with SH3 domains (12). It has been shown recently that ion channel subunits, displaying SH3 interaction domains, can function as "adaptor" proteins which allow Src-mediated phosphorylation of adjacent subunits otherwise unable to bind directly to Src (35). Among the HCN isoforms, only HCN1 possesses such a regulatory domain. Thus, heteromultimer assembly with HCN1 could specifically target signaling enzymes, such as Src, to subunits that would otherwise be inaccessible to these signals.

Upstream of the initiator codon of rbHCN1 cDNA we found a short ORF partly overlapping with rbHCN1 ORF. The cDNA sequence of this uORF is similar to the starting sequence of mouse HCN1 cDNA and indicates a recent divergence between the two species; a deletion seems to have occurred in rabbit which has generated a frameshift leading to a stop codon. uORFs are signs of translational control (36), and it has been reported previously that deletion or disruption of a uORF can stimulate downstream translation (37). We found that the presence of the uORF greatly reduces the fraction of transfected cells displaying rbHCN1 current (construct M1, Fig. 1*c*). We obtained a 20-fold higher fraction after disruption of the uORF sequence (construct M2), suggesting a regulatory role for this sequence in rbHCN1 translation. Reinitiation of translation at M3 after the uORF translation cannot be excluded, although our results (Fig. 1*c*) and the lack of analogy with the Kozak consensus sequence indicate that M3 is an inefficient initiator codon. Constructs M2 and M3 yielded indistinguishable currents, indicating that the first 29 amino acids of the N terminus do not affect channel behavior.

Data in the literature indicate a large variability in kinetic features of the different HCN isoforms and, more surprisingly, a certain degree of variability also among identical isoforms (16, 19, 20). Variability in parameters such as activation curve,

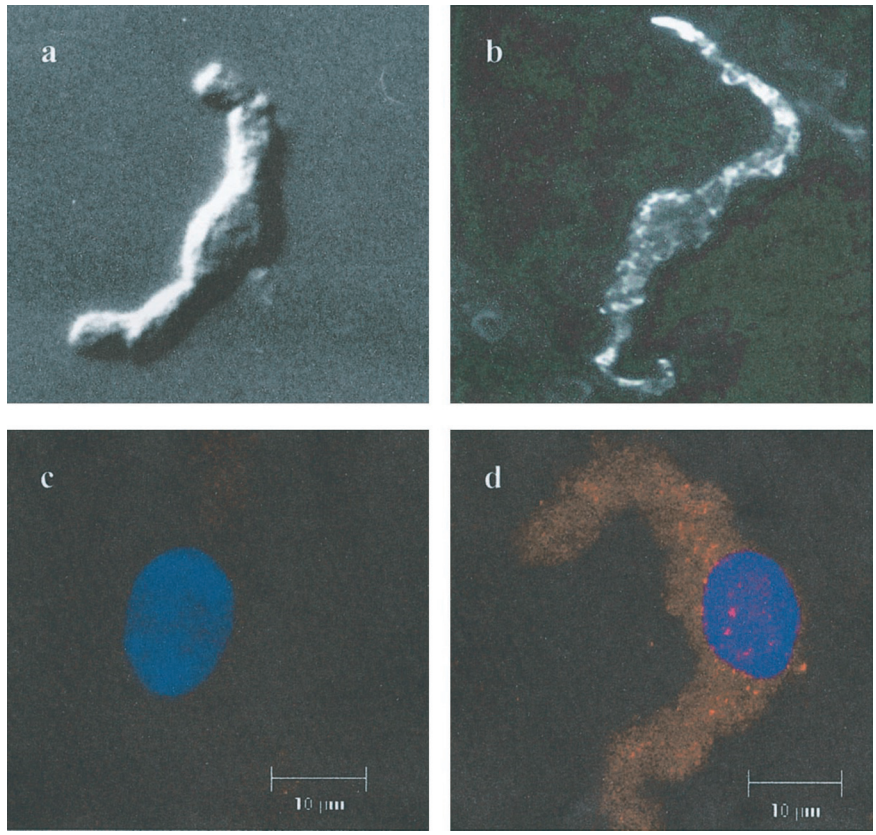

FIG. 7. **Immunolabeling of rabbit SAN myocytes with anti-neurofilament NF-M antibody iC8 and anti rb-HCN1 antibody αHCN1.** *Panel a*, typical morphology (prior to centrifugation and fixation) of a spindle-shaped pacemaker myocyte isolated from rbSAN. When tested by patch clamp, the I_f current is maximum in these myocytes. *Panel b*, SAN myocyte reacting with anti-neurofilament NF-L antibody. *Panel c*, control SAN myocyte. *Panel d*, SAN myocyte treated with αHCN1. *Red* staining corresponds to rhodaminated anti-rabbit antibody. The *blue circle* corresponds to the DAPI staining of the cell nucleus.

activation kinetics, and cAMP-induced shift thus appears to be affected by species, expression systems, experimental conditions, and protocols. We compared data from rbHCN1 and mHCN1 under similar experimental conditions, and we found that rbHCN1 activation kinetics was slower than that of mHCN1 despite the nearly identical activation curves (data not shown). For example, at −95 mV the activation time constants were 322 ms in rabbit and 101 ms in mouse HCN1, whereas the half-activation voltages were −73.4 mV in rabbit and −72 mV in mouse HCN1 (Table I and data not shown). In addition, the rbHCN1 current responded to cAMP with a 6.7 mV shift of the activation curve (Table I), a value higher than that reported for mHCN1 current (shift of 2 mV; Ref. 13). This implies that functionally relevant differences may exist among species despite high homology at the cDNA level.

The kinetics of rbHCN1 channels was severalfold faster than that of native I_f under similar conditions. At −95 mV the activation time constant was 1,068 ms in native SAN I_f measured at room temperature compared with 322 ms for rbHCN1 (Table I). Whereas the position of the activation curve of rb-HCN1 was comparable to that of native channels (Table I and Refs. 25, 23, 30, 38, 39), its response to cAMP was much reduced (3, 4, 40). Thus, kinetics and modulatory properties of rbHCN1 rule against the assumption that native rabbit I_f are simply HCN1 homomers. This does not exclude that HCN1 may contribute to the I_f current together with other HCN isoforms. Other than HCN4, which is strongly expressed in rabbit SAN, HCN1 is the isoform that according to previous data was expressed in appreciable amounts (21). It therefore seems possible that HCN1 contributes to the native current, for instance by accelerating the slow activation kinetics of rabbit HCN4 currents (Table I and Refs. 16, 18, 19). Our data indicate that the activation kinetics of the native channel, as well as the cAMP-induced shift, are intermediate between those of HCN1 and HCN4. In analogy with other voltage-gated potassium channels, HCN channels are probably tetramers, and it is possible that they form heteromultimers. Another possibility is that both clones contribute to I_f current by forming homomultimers. Two hyperpolarization-activated components with different kinetics have sometimes been described (16). The bradycardic zebrafish mutant *slo*, for example, lacked the fast component and expressed a slower component of the cardiac I_f current (41).

A major concern of our work has been to exclude the possibility that the presence of HCN1 in dissected SAN preparation was caused by neuronal contamination, particularly because SAN is highly innervated by autonomic nerve endings. The *in situ* results (Fig. 4) ruled against this possibility because the signal specifically accumulated in SAN and not in the conduction myocytes of the atrioventricular node and bundle, an equally well innervated region of the heart. The *in situ* data also showed specific expression of HCN1 in the SAN and lack of expression in other areas of the heart such as working atrial or ventricular myocytes.

It is tentative to speculate that the presence of HCN1 in SAN, but not in other regions of the heart, may reflect a specific HCN1 contribution to pacemaker current in this tissue, which is the natural leading pacemaker region where spontaneous activity is generated. To be able to generate and drive activity of the whole surrounding area, the intrinsic pacemaker rate is slightly higher in the "central" SAN region than in more peripheral regions (33). This function would be well served by the presence of an especially fast pacemaker current component such as the one supplied by HCN1.

Further evidence for specific localization in the SAN came from immunolocalization experiments performed on isolated SAN myocytes (Fig. 7). Although our preparation contained other types of cells (including transitional cells and atrial myocytes; not shown) the signal specifically accumulated in the spindle-type myocytes, where expression of I_f was highest in the SAN.

Our data do not allow us to establish whether the signal was

localized on the cell membrane or inside the cell. The antibody was raised against a cytoplasmic region of the channel and could thus recognize its epitope in any subcellular compartment of permeabilized cells.

In Western blot, αHCN1 recognized a prominent 50-kDa band in rabbit SAN, also present in hippocampus of rabbit and mouse (Fig. 6). This band corresponds roughly in mass to half of the HCN1 protein and could represent the large cytoplasmic domain, downstream of the six transmembrane segments. We observed a similar pattern in Western blot of mouse hippocampus for another HCN isoform, HCN2, using a commercially available antibody (Alomone, APC-030) that recognized, together with the expected 97-kDa band, an additional 50-kDa band (data not shown). A possible explanation is that this low mass band corresponds to a splice variant of the HCN clone. In rod photoreceptors, for example, a splice variant of the pore-forming β-subunit exists as a soluble form that interacts with signaling molecules in a macromolecular complex (42). Alternatively, this band may result from post-translational events that control the amount of functional protein. Such a mechanism would represent a way to modulate the contribution of HCN1 to the I_f current.

The finding that a protein (HCN1) considered to be specific for the nervous system is expressed in the SAN lends support to the hypothesis that SAN myocytes have an atypical set of expressed proteins, unlike myocytes of the working myocardium. Although most of them are the product of embryonic cardiac genes, a subset of proteins and epitopes is shared with neural tissue (31, 43, 44). Independent evidence for specific, neuronal-like protein expression is the observation that in newborn SAN, a neuronal type I fast sodium channel exists and is under developmental control (44).

In summary, our results identify rbHCN1 as one of the likely components of native I_f in the SAN myocytes of the rabbit heart. This raises the possibility that rbHCN1, together with other isoforms expressed in pacemaking cells (such as rbHCN4; 18) contributes to the assembly of heteromultimeric native cardiac I_f channels or to a mixed population of homomultimeric channels. The presence of a uORF and the potential control of transcriptional, translational, and post-translational events on the total amount of functional rbHCN1 protein may be relevant to determining the contribution of HCN1 to the pacemaker current I_f .

Acknowledgments—We thank U. Fascio and C. Ricci (University of Milan) for valuable help with confocal and differential interference contrast images, B. Santoro (Columbia University, New York) and H. Ohmori (University of Kyoto) for providing mBCNG1 and HAC4, and J. Dainty (Norwich) for reading the manuscript and for useful suggestions.

REFERENCES

1. Brown, H. F., DiFrancesco, D., and Noble, S. J. (1979) *Nature* **280,** 235–236
2. DiFrancesco, D. (1986) *Nature* **324,** 470–473
3. DiFrancesco, D. (1993) *Annu. Rev. Physiol.* **55,** 451–467
4. DiFrancesco, D., and Tortora, P. (1991) *Nature* **351,** 145–147
5. DiFrancesco, D., and Tromba, C. (1988) *J. Physiol.* (*Lond.*) **405,** 493–510
6. DiFrancesco, D. (1981) *J. Physiol.* (*Lond.*) **314,** 377–393
7. Earm, Y. E., Shimoni, Y., and Spindler, A. J. (1983) *J. Physiol.* (*Lond.*) **342,** 569–590
8. Yu, H., Chang, F., and Cohen, I. S. (1995) *J. Physiol.* (*Lond.*) **485,** 469–483
9. Pape, H. C. (1996) *Annu. Rev. Physiol.* **58,** 299–327
10. Luthi, A., and McCormick, D. A. (1998) *Neuron* **21,** 9–12
11. Clapham, D. E. (1998) *Neuron* **21,** 5–7
12. Santoro, B., Grant, S. G. N., Bartsch, D., and Kandel, E. R. (1997) *Proc. Natl. Acad. Sci. U. S. A.* **94,** 14815–14820
13. Santoro, B., Liu, D. T., Yao, H., Bartsch, D., Kandel, E. R, Siegelbaum, S. A, and Tibbs, G. R. (1998) *Cell* **93,** 717–729
14. Gauss, R., Deifert, R., and Kaupp, U. B. (1988) *Nature* **393,** 583–587
15. Ludwig, A., Zong, X., Jeglitsch, M., Hofmann, F., and Biel, M. (1998) *Nature* **393,** 587–591
16. Ludwig, A., Zong, X., Stieber, J., Hullin, R., Hofmann, F., and Biel, M. (1999) *EMBO J.* **9,** 2323–2329
17. Vaccari, T., Moroni, A., Rocchi, M., Gorza, L., Bianchi, M. E., Beltrame, M., and DiFrancesco, D. (1999) *Biochim. Biophys. Acta* **1446,** 419–425
18. Ishii, T. M., Takano, M., Xie, L. H., Noma, A., and Ohmori, H. (1999) *J. Biol. Chem.* **274,** 12835–12839
19. Seifert, R., Scholten, A., Gauss, R., Mincheva, A., Lichter, P., and Kaupp, U. B. (1999) *Proc. Nat. Acad. Sci. U. S. A.* **96,** 9391–9396
20. Moroni, A., Barbuti, A., Altomare, C., Viscomi, C., Morgan, J., Baruscotti, M., and DiFrancesco, D. (2000) *Pflügers Arch. Eur. J. Physiol.* **439,** 618–626
21. Moroni, A., Vaccari, T., Bianchi, M. E., Beltrame, M., and DiFrancesco, D. (1999) *Biophys. J.* **76,** 210 (abstr.)
22. Shi, W., Wymore, R., Yu, H., Wu, J., Wymore, R. T., Pan, Z., Robinson, R. B., Dixon, J. E., McKinnon, D., and Cohen, I. S. (1999) *Circ. Res.* **85,** e1–e6
23. Van Ginneken, A. C. G., and Giles, W. (1991) *J. Physiol.* (*Lond.*) **434,** 57–83
24. DiFrancesco, D., Noble, D. (1989) in *Neuronal and Cellular Oscillators* (Jacklet, J. W., ed) pp. 31–57, Marcel Dekker, New York
25. DiFrancesco, D., Ferroni, A., Mazzanti, M., and Tromba, C. (1986) *J. Physiol* (*Lond.*) **377,** 61–68
26. Kozak, M. (1987) *J. Mol. Biol.* **196,** 947–950
27. Simpson, L., and Emeson, R. B. (1996) *Annu. Rev. Neurosci.* **19,** 27–52
28. Kinsella, T. M., and Nolan, P. G. (1996) *Hum. Gene Ther.* **7,** 1405–1413
29. Zaza, A., Robinson, R. B., and DiFrancesco, D. (1996) *J. Physiol.* (*Lond.*) **491,** 347–355
30. Accili, E. A., and DiFrancesco, D. (1996) *Pflügers Arch. Eur. J. Physiol.* **431,** 757–762
31. Vitadello, M., Vettore, S., Lamar, E., Chien, K. R., and Gorza, L. (1996) *J. Mol. Cell. Cardiol.* **28,** 1833–1844
32. Gorza, L., and Vitadello, M. (1989) *Circ. Res.* **65,** 360–369
33. Masson-Pévet, M., Bleeker, W. K., Mackaay, A. J. C., Bouman, L. N., and Houtkooper, J. M. (1979) *J. Mol. Cell. Cardiol.* **11,** 555–568
34. Verheijck, E. E., Wessels, A., van Ginneken, A., Bourier, J., Markman, M. W., Vermeulen, J. L., de Bakker, J. M., Lamers, W. H., Opthof, T., and Bouman, L. N. (1998) *Circulation* **97,** 1623–1631
35. Nitabasch, M. N., Llamas, D. A., Araneda, R. C., Intile, J. L., Thompson, I. J., Zhou, Y. I., and Holmes, T. C. (2001) *Proc. Natl. Acad. Sci. U. S. A.* **98,** 705–710
36. Kozak, M. (1991) *J. Cell Biol.* **115,** 887–903
37. Damiani, R. D., and Wessler, S. R. (1993) *Proc. Natl. Acad. Sci. U. S. A.* **90,** 8244–8248
38. Denyer, J. C., and Brown, H. F. (1990) *J. Physiol.* (*Lond.*) **428,** 405–424
39. Hagiwara, N., and Irisawa, H. (1989) *J. Physiol.* (*Lond.*) **409,** 121–141
40. DiFrancesco, D., and Mangoni, M. (1994) *J. Physiol.* (*Lond.*) **474,** 473–482
41. Baker, K., Warren, K. S., Yellen, G., and Fishman, M. C. (1997) *Proc. Natl. Acad. Sci. U. S. A.* **94,** 4554–4559
42. Körschen, H. G., Beyermann, M., Müller, F., Heck, M., Vantler, M., Koch, K., Kellner, R., Wolfrum, U., Bode, C., Hofmann, K. P., and Kaupp, U. B. (1999) *Nature* **400,** 761–766
43. Moorman, A. F., de Jong, F., Denyn, M. M., and Lamers, W. H. (1998) *Circ. Res.* **82,** 629–644
44. Baruscotti, M., Westenbroek, R., Catterall, W. A., DiFrancesco, D., and Robinson, R. B. (1997) *J Physiol.* (*Lond.*) **498,** 641–648
45. Bois, P., Renaudon, B., Baruscotti, M., Lenfant, J., and DiFrancesco, D. (1997) *J. Physiol.* (*Lond.*) **501,** 565–571